Substrate strain and doping effects on the crystal structure of SrNbxTi1–xO3

Luis Dacal, Andres Cantarero, Valerio Olevano

Eur. Phys. J. B (2019) 92: 181
https://doi.org/10.1140/epjb/e2019-100120-4

THE EUROPEAN PHYSICAL JOURNAL B

Regular Article

Substrate strain and doping effects on the crystal structure of $SrNb_xTi_{1-x}O_3$

Luis C.O. Dacal[1,a], Andres Cantarero[2], and Valerio Olevano[3,4]

[1] Instituto de Estudos Avançados, IEAv-CTA, P.O. Box 6044, 12228-970 São José dos Campos – SP, Brazil
[2] Molecular Science Institute, Universitat de València, P.O. Box 22985, 46071 Valencia, Spain
[3] Université Grenoble Alpes, 38000 Grenoble, France
[4] European Theoretical Spectroscopy Facility (ETSF) and CNRS, Institut Néel, 38042 Grenoble, France

Received 28 February 2019 / Received in final form 10 June 2019
Published online 12 August 2019

Abstract. Strontium titanate, $SrTiO_3$ (STO), is an interesting material for both fundamental studies and technological applications. Modifications of the atomic and crystal structure by doping, e.g. replacing titanium with niobium atoms, and by strain, i.e. by growing STO on a different substrate such as lanthanum aluminate, $LaAlO_3$ (LAO), have been proposed to tune the STO electronic, optical and transport properties for applications. Here we report the results of ab initio density-functional theory (DFT) simulations of both strain and Nb-doping effects, independently and joint, on the STO crystal structure. We found that the DFT energy differences among the three commonly observed STO crystal structures, $Pm\bar{3}m$, $P4/mmm$, and $I4/mcm$, are very small, $<2.6\times10^{-4}$ Ry, so that the ground-state cannot be determined unambiguously at this level of theory and physics. Our calculations show that an in-plane strain, at least at the level of only -0.4% as observed in STO on LAO, does not lead to the expected increase in c toward tetragonal symmetry, where c is the length of the cell axis perpendicular to the plane. Instead, c also is reduced and the cubic symmetry tends to be restored. Nb doping, even at the maximum experimental level of 3.7%, does not have significant effects on lattice parameters. The latter result is confirmed also under the presence of strain, so we could not find any crossed effect of strain and doping.

1 Introduction

The perovskite-type $SrTiO_3$ (STO) is a system which has attracted considerable interest both for being a model transition-metal oxide to study and understand fundamental physics [1–4], and also for the use of its electronic, optical and transport properties in technological applications, for example in the development of new devices [5]. STO heterostructures with other oxides, in particular combining STO with $LaAlO_3$ (LAO), has also been found to present surprising effects [6–10], like magnetotransport occurring at the STO/LAO interface [6], though the most investigated property is the electrical conductance [7–11] for its relevance in devices.

Fundamental in technological applications is the ability to control and tune material properties. Strain of the atomic structure, as by growing STO on a different substrate, is one possibility: it can induce modifications in the crystal structure with consequences on electronic, optical, and transport properties. LAO is again the most common choice for a substrate to STO, the LAO induced strain distribution has been investigated on samples grown under special conditions [12]. The relationship between strain and phase transitions has also been investigated in STO samples grown on a buffer layer of $SrRuO_3$ [13]. The analysis has been pushed up to study the relation between strain and thermoelectric [14] or electronic [15] properties, though the investigated tensile and compressive strains were of the order of 1%, so beyond the possibility to effectively grow the corresponding samples.

Doping is another way to control and tune STO properties. The effects of doping, as by replacing titanium by niobium atoms, on the thermoelectric performance of $SrTi_{1-x}Nb_xO_3$ (SNTO) were experimentally [16,17] and theoretically investigated [18], though in the latter a too high, $x = 12.5\%$, doping level was considered. Other studies have evidenced the role played by the localized d-electrons in excitons, with important correlation effects on electronic, optical, and transport properties [19–22]. From the structural point of view there are also SNTO studies on dislocations [23], on the crystal homogeneity [24], and finally on defects and their influence on magnetotransport properties [25].

This work is an ab initio density-functional theory (DFT) study of the effects on the STO crystal structure of the application of a biaxial strain to simulate STO thin

[a] e-mail: lcodacal@gmail.com

films grown on a different substrate like LAO. At the same time, we also study the effects of doping by niobium, as in SNTO, both independently and jointly with strain. We consider realistic values for both strain, e.g. −0.4866% for STO on LAO [26], and also doping, achieving down the level of $x = 3.7\%$, much closer to realistic values though requiring a more important computational effort. In order to understand our results and have comparison terms, we first studied the pristine bulk most common crystal structures, i.e. cubic $Pm\bar{3}m$, tetragonal $P4/mmm$, and finally $I4/mcm$, for unstrained and undoped STO, as well as for the doping diagram opposite side, $SrNbO_3$ (SNO).

2 Method

We have performed ab initio DFT calculations of the STO crystal structure under different conditions by an all-electron full-potential linearized augmented plane-wave (AE-FP-LAPW) method, as implemented in the Wien2K code [27]. It is important to say that the differences among the total energies of the three STO crystal structures we considered here are of the order of 0.1 mRy and can achieve even 10^{-2} mRy (0.1 meV). A recent work comparing the maximum accuracy achieved by DFT methods [28] has clarified that only AE-FP-LAPW methods can achieve such accuracies, and the accuracy reduces when passing to PAW, USPP and at last NCPP methods as shown in its Figure 4. When changing pseudopotential, the total energy can change by one meV or more. So that, in cases where the difference between two crystal structures is less than this, it is better to always check the result by using AE-FP-LAPW methods. Because of this, all the results quoted here refer to the AE-FP-LAPW approach, and so are free from possible bias by different choices of pseudopotentials and can be used as reference for other calculations.

The local density approximation (LDA) [29] has been employed in all calculations, but some structural effects were double checked with the Perdew-Burke-Ernzerhof (PBE) [30] generalized-gradient approximation (GGA).

Since the explicit inclusion of the substrate layer in our model would make the calculations intractable, we have simulated the strain in STO thin films grown on a different substrate by forcing the a in plane lattice parameter of the bulk STO structure to assume reduced values, while relaxing all the other parameters of the crystal structure. A very accurate experiment [26] have measured the reduction of the a parameter to be −0.4866% for STO grown on LAO. In other words, in our model, the structural effects of the substrate on the STO thin layer will be represented by the corresponding in plane strain value, that is −0.4866% for STO grown on LAO. On the other hand the doping was simulated as in the real situation, by replacing one Ti atom by one Nb in larger cells, up to the $3 \times 3 \times 3$ supercell, such as to approach the maximum available experimental doping levels ($2 \sim 3\%$).

The ranges of the main input parameters employed in our calculations are shown in Table 1, where RMT-X stands for the "muffin-tin" radius of the corresponding "X" element, $RK_{\max}$ is the product between the smallest atomic muffin-tin radius and the magnitude of the largest K vector of the plane-wave basis set, N_k is the number of inequivalent k-points in the irreducible wedge of the Brillouin zone, and E_{cut} is the energy that separates core and valence electronic states. All our calculated relaxed lattice parameters are converged to less than 0.1%.

Table 1. Ranges for the main input parameters. See text for details.

Parameter	Minimum	Maximum
RMT-Sr (Bohr)	1.80	2.50
RMT-Nb (Bohr)	1.63	1.89
RMT-Ti (Bohr)	1.57	1.85
RMT-O (Bohr)	1.42	1.71
$RK_{\max}$	7.0	7.5
N_k	4	30
E_{cut} (Ry)	−6.0	−6.0

3 Results

3.1 Unstrained and undoped $SrTiO_3$ and $SrNbO_3$

The crystal structure of $SrNbO_3$ (SNO) is known to be cubic [31]. However, in order to have comparable results between STO and SNO, for both we optimize the cells corresponding to the $Pm\bar{3}m$, $P4/mmm$, and $I4/mcm$ space groups. The main purpose to study SNO is to get some insights on the structural effects of the Nb doping on the STO atomic structure.

In Table 2 we show our LDA results, both energies and lattice parameters, for the three different crystal symmetries for both STO and SNO. We also show the corresponding heats of formation calculated at ambient pressure and taking the cubic phase as the energy origin. One can see that the cubic crystal structure is clearly the lowest energy for SNO. On the other hand, in the case of STO and despite reducing the energy convergence criterion to 10^{-5} Ry, one cannot unambiguously state which crystal structure is the most stable. However, the energies are equal within the assumed convergence error, and the optimized structural parameters for the $P4/mmm$ STO cell are practically the same as that obtained for the $Pm\bar{3}m$ structure. So that we can state that both optimization processes lead to the same cell. In the case of the $I4/mcm$ space group, the unit cell parameter a (xy plane) must be divided by $\sqrt{2}$ and c (z axis) by 2 in order to compare them with the other cells results. This means that we have an *effective* $a = 7.319$ Bohr and an *effective* $c = 7.317$ Bohr, a little bit farther from the STO cubic result. Starting from the $I4/mcm$ structure, cell optimization tends to revoke TiO_6 octahedra rotations, thus leading to the $P4/mmm$ space group where octahedra are aligned. To a lesser extent, cell optimization also tends to nullify the c and a lattice parameter difference, thus leading the tetragonal to the cubic symmetry. We can conclude that our calculations provide the cubic $Pm\bar{3}m$ as the most stable structure. This behavior was double checked using LDA and GGA PBE. Our results are in agreement with the experiment for bulk SNO, but not for

Table 2. Optimized LDA structural parameters in atomic units (Bohr) and the corresponding energies (Ry) and heats of formation (cal/mol) of the three different phases analyzed here for STO (top panel) and SNO (bottom panel).

Space group	a (Bohr)	c (Bohr)	Energy (Ry)	Heat of formation (cal/mol)
			STO	
$Pm\bar{3}m$	7.297		−17012.04506	0
$P4/mmm$	7.300	7.292	−17012.04507	−3
$I4/mcm$	10.350	14.633	−17012.04481	78
			SNO	
$Pm\bar{3}m$	7.552		−28869.5500	0
$P4/mmm$	7.595	7.411	−28869.5442	1819
$I4/mcm$	10.688	15.116	−28868.9462	189318

Table 3. Cubic ($Pm\bar{3}m$ space group) a lattice parameter in Bohr, for both STO and SNO. We report the theoretical relaxed LDA and GGA PBE lattice parameters, as well as the experimentally measured [26,31].

a (Bohr)	STO	SNO
LDA	7.297	7.552
EXP	7.379	7.604
PBE	7.457	

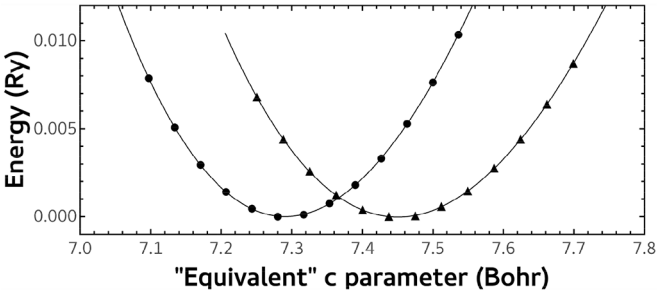

Fig. 1. Total energy versus the lattice parameter c for the $I4/mcm$ $SrTiO_3$ cell including in plane strain and using the LDA (circles) and GGA PBE (triangles) exchange-correlation approximations. The continuous lines represent Murnaghan fits to find the minima. The a parameter is fixed and taken at the bulk unstrained value reduced by a −0.4866% to account for the LAO substrate. The c parameter refers not to the $I4/mcm$, but to the conventional tetragonal $P4/mmm$ cell. The energy origin was redefined for clarity. The fitted curves show the following optimized c values: 7.291 Bohr (LDA) and 7.450 Bohr (GGA PBE).

bulk STO where it is experimentally known that the most stable cell (the low temperature phase) is the $I4/mcm$ one [26]. We believe that this disagreement may be a manifestation of the Jahn-Teller effect [32], that favors a structure distortion and reduces the symmetry of the ground state crystal cell. In this case, neither LDA nor GGA-PBE were able to capture this well knonw but small effect.

Finally, the comparison between the STO and SNO cubic cells (Tab. 3) shows that the a parameter is almost 3.5% larger in SNO than in STO. This is an expected result since the Nb atom is bigger than the Ti one. Hence, some distortion in the STO lattice should occur when it is doped with Nb. Indeed, experimental results show this behavior in solid solution samples with LAO substrate, but only for Nb concentrations higher than 50% [33]. It is important to say that, in this work, we did not analyze solid solutions, but single crystal SNTO samples grown on LAO substrates.

3.2 Strain effects

The explicit inclusion of the substrate would require the inclusion of a number of substrate layers sufficient to achieve LAO bulk properties, which means large supercells and a non-linear increase in the computational cost. This is needed if the purpose is to study the STO/LAO interface and the associated physics. Since here we are not interested in interface physics and we just want to study the effect of the LAO substrate on the STO crystal structure, with possible consequences on the electronic properties, we only take into account the LAO substrate biaxial strain effect on STO and do not include any LAO layer in the simulation. Therefore we have performed simulations of the LAO effect on STO by imposing a −0.4866% reduction on the STO a lattice parameter as measured experimentally [26]. Notice that, in order to simulate an effective strain, the reduction has to be applied not on the experimental, and rather on the theoretical relaxed a values which depends on the DFT functional (LDA or PBE) used. Hence, the reduction was applied on top of the LDA bulk relaxed a, which, as usual, underestimates the experimental value, and on top of the GGA PBE a, which, on the other side, overestimates it (Tab. 3). Notice that the strain reduction is smaller than the lattice parameter difference between LDA and PBE. So, the strategy to perform calculations in both LDA and GGA allows us to validate strain effects and behaviors that are only checked by both approximations. The calculations were performed starting from the $I4/mcm$ crystal structure. The a lattice parameter was kept fixed at the strained value and we performed a dozen calculations exploring different c values. In each calculation we started from a $I4/mcm$ atomic structure with rotated TiO_6 octahedra and we let relax the octahedra angles (θ) and all $I4/mcm$ internal atomic parameters.

In Figure 1 we show the total energy versus the c lattice parameter for strained STO $I4/mcm$ cells for both LDA (left curve) and GGA (right). We also show the Murnaghan fitting curves which have a good overlap with the calculated total energy points, confirming the validity

and reliability of our results and conclusions. In principle, when shrinking a one would expect a proportional stretch of c so to conserve the cell volume at first order. In contrast, our results show that this is not the case for strained STO. We rather found a *shrinking* of c as well. And this is confirmed by LDA and GGA calculations. We found $c = 7.291$ Bohr in LDA and $c = 7.450$ Bohr in GGA PBE, to be compared with the corresponding unstrained bulk values (Tab. 2 for LDA). The shrinking found on c is smaller than the shrinking imposed on a. Moreover, also in presence of strain the relaxation of internal atomic parameters leads TiO_6 octahedra to realign, that is the rotation angle θ tends to zero. This behavior was observed in both LDA and GGA calculations, and in all the range of c parameters we have explored.

In conclusion, we can claim that a biaxial strain induced by the LAO substrate on the STO a parameter, has not the expected effects on the STO crystal structure: it does not enforce tetragonality, that is an increase of c, and rather it tries to restore the cubic $Pm\bar{3}m$ symmetry by both reducing c and also realigning TiO_6 octahedra towards the $\theta \to 0$ value of the more symmetric space groups.

We have here to mention a work by Lebedev using the Pseudopotentials method [34] which analyzed tensile strain effects on STO, finding a rich evolution of its crystal symmetry. However, he/she explored a range of strains different from that one addressed here.

3.3 Nb doping effects

We remind that for bulk STO we have not found the crystal structure $I4/mcm$ more stable than the cubic. This is more so for SNO. Moreover, the SNO cubic phase is experimentally stable at ambient and even low temperature. So, it is reasonable to expect that doping STO by Nb cannot affect the STO $Pm\bar{3}m$ versus $I4/mcm$ phase stability order. For this reason, Nb doping effects were simulated by building STO cubic supercells and replacing one Ti atom by a Nb one. It is important to realize that the Ti atom occupy the vertice sites of the cubic STO cell. This means that no matter what Ti atom we change by Nb, there will not be artifacts created by the Nb position. This is also valid in the case of the tetragonal STO cells. We typically used a $3 \times 3 \times 3$ STO supercell that contains 27 elementary STO cells. In this supercell we replaced one of the 27 Ti atoms by one Nb atom, getting a Nb-doping level of $x = 1/27 \sim 3.7\%$. Here, it is important to stress that this means a real calculation on the $SrNb_xTi_{1-x}O_3$ system, which is the most realistic simulation of doping, much better than taking an elementary cell of STO and simply adding/removing extra electrons.

In Figure 2 we show both the LDA and GGA optimization of the lattice parameter a referred to the conventional $1 \times 1 \times 1$ cell but, of course, carried on in the supercell geometry. Under Nb doping one can notice a small increase in the lattice parameter with respect to undoped STO (compare Tabs. 3 and 4). The increase is 0.18% in LDA, and slightly smaller, 0.15%, in GGA. We compare this with the increase of the lattice parameter of 3.5% when passing from pure STO to SNO (Tab. 3). So, under a level of an already high 3.7% Nb doping (though still in the range of real samples), we found an expected increase of the crystal cell, but not so significant as we hoped. We also tried a $2 \times 2 \times 2$ supercell, corresponding to an Nb doping of 12.5% much higher than the experimentally synthetized samples, and we found an increase of the a parameter of 0.47%. This is a more consistent modification of the crystal structure, but unfortunately at a level of doping which might not be any more of interest for technological applications.

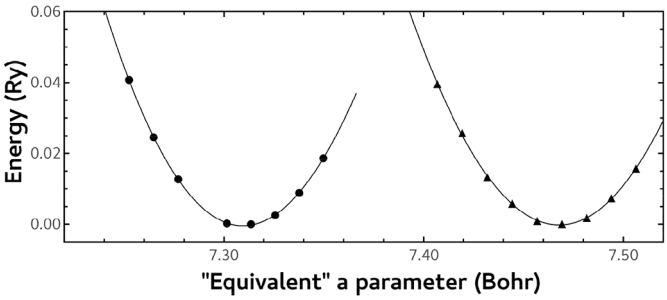

Fig. 2. Total energy versus lattice a parameter for 3.7% Nb-doped $SrNb_{0.037}Ti_{0.963}O_3$ cubic cell using the LDA (circles) and GGA PBE (triangles) exchange-correlation approximations. The continuous line represent a Murnaghan fit to find the minima. The energy origin was redefined for clarity. The a parameter refers not to the supercell, but to the simple cell.

Table 4. Lattice a parameter (Bohr) for cubic Nb-doped STO at the level of 3.7% and 12.5% in LDA and GGA PBE approximations. The a parameter refers not to the supercell, but to the simple $1 \times 1 \times 1$ cell.

SNTO relaxed a (Bohr)		
Nb doping	3.7%	12.5%
LDA	7.310	7.331
PBE	7.468	

3.4 Crossed strain and doping effects

Our last task was to check crossed strain and doping effects. Again, for the considerations discussed above and the results we have already found separately for strain and Nb-doping, it is reasonable to expect that the joint effect of strain and Nb doping cannot introduce TiO_6 octahedra rotation and favor the $I4/mcm$ crystal structure. Indeed, we have carefully investigated the possibility of octahedra rotation in between bulk unstrained and strained pure STO. This because the energy difference between the three crystal structures, namely $I4/mcm$, $Pm\bar{3}m$ and $P4/mmm$, is very small in pure STO (see Tab. 2). This is not the case in SNO where the octahedra rotated $I4/mcm$ structure is much higher in energy, and so strongly unfavored (see, again, Tab. 2). Hence, we expect that the doping of STO by replacement one Ti by one Nb atom, has the effect to further unfavor octahedra rotation, as it happens in SNO. Consequently, for joint Nb-doped and strained STO, we excluded the $I4/mcm$ crystal structure from our simulations. Nevertheless, we build for this case

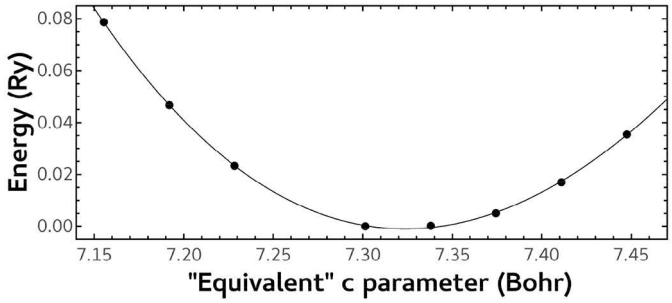

Fig. 3. Total energy versus lattice c parameter for $SrNb_{0.037}Ti_{0.963}O_3$ tetragonal cell including in plane strain and using the LDA exchange-correlation approximation. The continuous line is the Murnaghan fit to get the minimum. The a parameter is fixed to the optimized cubic cell value decreased by the experimental factor −0.4866%. The energy origin was redefined for clarity. The c parameter refers not to the supercell, but to the simple tetragonal cell.

Table 5. Lattice c parameter (Bohr) for 3.7% Nb-doped and −0.4866% LAO-strained STO. The lattice parameter refers not to the supercell, but to the simple $1 \times 1 \times 1$ cell.

SNTO (3.7% Nb) on LAO	Relaxed c (Bohr)
LDA	7.324

tetragonal supercells, using the experimentally measured relative value (−0.4866% [26]) to strain the theoretical relaxed a, letting c to relax, so to minimize the total energy. We again refer to the $3 \times 3 \times 3$ STO supercell corresponding to $SrNb_{0.037}Ti_{0.963}O_3$ and 3.7% Nb doping level.

In Figure 3 we report a structural optimization similar to Figure 2 for the doped and unstrained case, but this time the total energy is plot as a function of the c lattice parameter, being a fixed to the experimentally measured strain. Our calculations give for the optimized c an expected increase (Tab. 5). The optimized value is 0.19% greater than the lattice parameter for the doped-only $SrNb_{0.037}Ti_{0.963}O_3$ cubic system (Tab. 4). As already observed in the strain-only case, an increase of almost 1% in c is needed to conserve the volume of the unstrained cubic $SrNb_{0.037}Ti_{0.963}O_3$. The observed increase in c is again much less than expected. Even comparing with the the optimized $Pm\bar{3}m$ STO cell, the c parameter increase is negligible (smaller than 0.4%).

We can say in conclusion that, even when taken together, LAO strain and Nb doping do not affect considerably the STO crystal structure, so to alter sensibly its properties.

4 Conclusions

We presented a theoretical study of the biaxial in-plane compressive substrate strain and Nb-doping effects on the STO crystal structure. We simulated both strain and doping levels that are experimentally considered. More specifically, we considered an in-plane cell parameter with −0.4866% strain, as experimentally measured for STO grown on a LAO substrate. By using a direct supercell approach, we brute-force simulated a 3.7% Nb doping level which is an experimental reached value. The strain and doping effects were investigated both separately and jointly.

Our results show that both Nb-doping and strain have negligible effects on the STO crystal structure. Even when considered jointly, the effects are smaller than expected. The effects start to be considerable only at the level of 12.5% Nb doping, well beyond the range of experimentally considered dopings.

Here, we would like to highlight that despite the fact that changing the substrate material and / or doping element would mean simple changes of input parameters in our calculations, the so far obtained results, which show that noticeable effects demand experimentally unreachable values for strain and doping, do not justify the computational cost required to perform an extensive mapping of different substrate materials and doping elements.

In conclusion, from one side our work shows that doping and strain have weak tuning effects on STO. From the positive side, there is plenty of room for experimental manipulation of SNTO structures without destroying its thermoelectric properties and quantum transport.

Pierre Darancet (Center for Nanoscale Materials, Argonne National Laboratory – USA) is acknowledged for helpful discussions. This work was performed, in part, at the Center for Nanoscale Materials, a U.S. Department of Energy Office of Science User Facility, and supported by the U.S. Department of Energy, Office of Science, under Contract No. DE-AC02-06CH11357. Part of this work was also performed at CENAPAD-SP (Centro Nacional de Processamento de Alto Desempenho em São Paulo), project: UNICAMP / FINEP – MCT. This work was financially supported thorough grant: 2017/02045-2, São Paulo Research Foundation (FAPESP) and by the "Dirección General de Investigación científica y Técnica" of Spain through the grant MAT2016-63955-R.

Author contribution statement

A. Cantarero proposed the issue. L. Dacal performed the calculations. V. Olevano contributed to the analysis of data. All the three authors discussed the strategies and the results and wrote the paper.

References

1. V. Martelli, J.L. Jiménez, M. Continentino, E. Baggio-Saitovitch, K. Behnia, Phys. Rev. Lett. **120**, 125901 (2018)
2. W.D. Rice, P. Ambwani, M. Bombeck, J.D. Thompson, G. Haugstad, C. Leighton, S.A. Crooker, Nat. Mater. **13**, 481 (2014)
3. B. Himmetoglu, A. Janotti, H. Peelaers, A. Alkauskas, C.G.V. de Walle, Phys. Rev. B **90**, 241204 (2014)
4. G. Gupta, T. Nautiyal, S. Auluck, Phys. Rev. B **69**, 052101 (2004)

5. S. Wu, X. Luo, S. Turner, H. Peng, W. Lin, J. Ding, A. David, B. Wang, G.V. Tendeloo, J. Wang, T. Wu, Phys. Rev. X **3**, 041027 (2013)
6. V.K. Guduru, A. McCollam, A. Jost, S. Wenderich, H. Hilgenkamp, J.C. Maan, A. Brinkman, U. Zeitler, Phys. Rev. B **88**, 241301 (2013)
7. E. Breckenfeld, N. Bronn, J. Karthik, A.R. Damodaran, S. Lee, N. Mason, L.W. Martin, Phys. Rev. Lett. **110**, 19604 (2013)
8. Z.Q. Liu, C.J. Li, W.M. Lu, X.H. Huang, Z. Huang, S.W. Zeng, X.P. Qiu, L.S. Huang, A. Annadi, J.S. Chen, J.M.D. Coey, T. Venkatesan, Ariando, Phys. Rev. X **3**, 021010 (2013)
9. A. Ron, Y. Dagan, Phys. Rev. Lett. **112**, 136801 (2014)
10. M. Tomczyk, G. Cheng, H. Lee, S. Lu, A. Annadi, J.P. Veazey, M. Huang, P. Irvin, S. Ryu, C.B. Eom, J. Levy, Phys. Rev. Lett. **117**, 096801 (2016)
11. P. Lee, V. Singh, G. Guo, H.J. Liu, J.C. Lin, Y.H. Chu, C. Chen, M.W. Chu, Nat. Commun. **7**, 12773 (2016)
12. G. Panomsuwan, O. Takai, N. Saito, Appl. Phys. Lett. **105**, 051911 (2014)
13. F. He, B.O. Wells, Z.G. Ban, S.P. Alpay, S. Grenier, S.M. Shapiro, W. Si, A. Clark, X.X. Xi, Phys. Rev. B **70**, 235405 (2004)
14. D. Zou, Y. Liu, S. Xie, J. Lin, J. Li, Chem. Phys. Lett. **586**, 159 (2013)
15. A. Janotti, D. Steiauf, C.G.V. de Walle, Phys. Rev. B **84**, 201304 (2011)
16. S. Ohta, T. Nomura, H. Ohta, K. Koumoto, J. Appl. Phys. **97**, 034106 (2005)
17. J.D. Baniecki, M. Ishii, H. Aso, K. Kobayashi, K. Kurihara, K. Yamanaka, A. Vailionis, R. Schafranek, Appl. Phys. Lett. **99**, 232111 (2011)
18. J.D. Baniecki, M. Ishii, H. Aso, K. Kurihara, D. Ricinschi, J. Appl. Phys. **113**, 013701 (2013)
19. P.K. Gogoi, L. Sponza, D. Schmidt, T.C. Asmara, C. Diao, J.C.W. Lim, S.M. Poh, S.i. Kimura, P.E. Trevisanutto, V. Olevano, A. Rusydi, Phys. Rev. B **92**, 035119 (2015)
20. L. Sponza, V. Véniard, F. Sottile, C. Giorgetti, L. Reining, Phys. Rev. B **87**, 235102 (2013)
21. F. Sottile, M. Marsili, V. Olevano, L. Reining, Phys. Rev. B **76**, 161103 (2007)
22. T. Rangel, A. Ferretti, P.E. Trevisanutto, V. Olevano, G.M. Rignanese, Phys. Rev. B **84**, 045426 (2011)
23. J. Chen, T. Sekiguchi, J. Li, S. Ito, W. Yi, A. Ogura, Appl. Phys. Lett. **106**, 102109 (2016)
24. C. Rodenbücher, M. Luysberg, A. Schwedt, V. Havel, F. Gunkel, J. Mayer, R. Waser, Sci. Rep. **6**, 32250 (2016)
25. A. Sarantopoulos, E. Ferreiro-Vila, V. Pardo, C. Magén, M.H. Aguirre, F. Rivadulla, Phys. Rev. Lett. **115**, 166801 (2015)
26. F. He, B.O. Wells, S.M. Shapiro, Phys. Rev. Lett. **94**, 176101 (2005)
27. P. Blaha, K. Schwarz, G.K.H. Madsen, D. Kvasnicka, J. Luitz, *WIEN2k, An Augmented Plane Wave + Local Orbitals Program for Calculating Crystal Properties* (Karlheinz Schwarz, Techn. Universität Wien, Austria, 2001)
28. K. Lejaeghere, et al., Science **351**, aad3000 (2016)
29. J.P. Perdew, Y. Wang, Phys. Rev. B **45**, 13244 (1992)
30. J.P. Perdew, S. Burke, M. Ernzerhof, Phys. Rev. Lett. **77**, 3865 (1996)
31. S.A. Turzhevsky, D.L. Novikov, V.A. Gubanov, A.J. Freeman, Phys. Rev. B **50**, 3200 (1994)
32. H.A. Jahn, E. Teller, Proc. R. Soc. Lond. A **161**, 220 (1937)
33. Y. Zhang, B. Feng, H. Hayashi, T. Tohei, I. Tanaka, Y. Ikuhara, H. Ohta, J. Appl. Phys. **121**, 185102 (2017)
34. A.I. Lebedev, Phys. Solid State **58**, 300 (2016)